3) The wing boundary-layer thickness is equal to the wing-nacelle gap of $1D$ at the nacelle trailing edge when $\alpha = 0$ deg.

4) For the smallest gap, $0.5D$, the nacelle inlet is partially inside the wing boundary layer. At $\alpha = -2$ deg, some boundary layer enters the nacelle and distorts the nacelle exhaust flow symmetry. The amount of wing boundary layer flowing through the nacelle and the associated distortion are lessened with the increase of α.

Acknowledgment

This work was supported by NASA Ames Research Center under Contract A24888D(MXR).

References

[1]Rech, J., and Leyman, C. S., "Concorde Aerodynamics and Associated Systems Development," *A Case Study by Aerospatiale and British Aerospace on the Concorde*, AIAA Professional Study Series, Sec. 6, 1980, pp. 1–39.

[2]Carter, E. C., "Experimental Determination of Inlet Characteristics and Inlet and Airframe Interference," *Airframe/Engine Integration*, edited by A. Ferri, AGARD Lecture Series 53, Paper 3, May 1972, pp. 1–23.

[3]Leynaert, J., Surber, L. E., and Goldsmith, E. L., "Transport Aircraft Intake Design," *Practical Intake Aerodynamic Design*, edited by E. L. Goldsmith and J. Seddon, AIAA Education Series, AIAA, Washington, DC, 1993, pp. 218–231.

[4]Kuchemann, D., *The Aerodynamic Design of Aircraft*, Pergamon, Oxford, England, UK, 1978, pp. 56–102.

[5]Biber, K., "Calibration and Use of WSU 9 × 9-inch Supersonic Wind Tunnel," Wichita State Univ., NIAR Rept. 93-17, Wichita, KS, July 1993.

[6]Pope, A., and Goin, L. K., *High-Speed Wind Tunnel Testing*, Krieger, Malabar, FL, 1965, pp. 50–53.

[7]NASA Ames Research Staff, "Equations, Tables, and Charts for Compressible Flow," NACA Rept. 1135, 1953.

[8]Biber, K., and Ellis, D. R., "Supersonic Flow Visualization of a Nacelle in Close Proximity to a Simulated Wing," Wichita State Univ., NIAR Rept. 93-18, Wichita, KS, July 1993; also see AIAA Paper 94-0670, Jan. 1994.

[9]Shapiro, A. H., *The Dynamics and Thermodynamics of Compressible Fluid Flow*, Vol. I, Wiley, New York, 1953, pp. 170–173.

[10]Schlichting, H., *Boundary-Layer Theory*, 7th ed., McGraw-Hill, New York, 1979, pp. 24–46.

[11]Green, J. E., "Interactions Between Shock Waves and Turbulent Boundary Layers," *Progress in Aerospace Sciences*, Vol. 11, edited by D. Kuchemann, Pergamon, Oxford, England, UK, 1970, pp. 235–340.

Analytic Prediction of Lift for Delta Wings with Partial Leading-Edge Thrust

Lance W. Traub*
University of the Witwatersrand, Johannesburg, South Africa

Nomenclature

AR = aspect ratio, b^2/S
b = wing span
C_D = drag coefficient
C_{Di} = lift dependent drag coefficient
C_{Do} = zero lift drag coefficient
C_L = lift coefficient
C_N = attached flow normal force coefficient
C_{SE} = side-edge suction coefficient
C_T = theoretical wing thrust coefficient
$C_{T_{eff}}$ = overall leading-edge thrust coefficient
c = local wing chord
c_R = wing root chord
c_t = sectional theoretical thrust coefficient
k_i = induced drag constant
k_p = potential constant
r = leading-edge radius
S = wing area
α = angle of attack
η = nondimensional spanwise coordinate, $2y/b$
η_s = spanwise position at which the leading-edge drag equals the leading-edge thrust
η_T = spanwise position at which attainable thrust is equal to theoretical thrust
Λ_{LE} = leading-edge sweep angle
λ = taper ratio

Received Nov. 15, 1992; revision received July 19, 1993; accepted for publication Aug. 2, 1993.

*Graduate Student, School of Mechanical Engineering, Branch of Aeronautical Engineering, 1 Jan Smuts Ave., P.O. Wits, 2050.

Introduction

HIGH subsonic and supersonic flight has necessitated the use of thin slender wings to reduce drag. These wings are typically characterized by flow separation at low angles of attack. For slender wings the separated flow leads to the formation of leading-edge vortices which, in turn, give rise to additional nonlinear vortex lift. Polhamus[1,2] successfully accounted for this additional lift by means of a leading-edge suction analogy (where the leading-edge suction force is assumed to rotate through 90 deg and supplement the normal force coefficient). Bradley et al.[3] extended the analogy to include wings with curved leading edges. The theory of Polhamus predicts the overall force coefficients, but gives no indication of spanwise distributions. Purvis[4] derived analytic equations based on Polhamus' analogy to predict the characteristics of sharp-edged generalized planforms by determining an expression for their leading-edge thrust distribution. Some computational techniques that model slender wings use the suction analogy and model the lifting surface using a vortex lattice,[5] whereas others model the wake using discrete load-free filaments.[5] Although the suction analogy is successful, the influence of the aerofoil geometry and its effects on the amount of leading-edge thrust developed (or the attainable thrust) is not accounted for. It is assumed that the leading edge is sharp and that flow separation is total, so that no leading-edge thrust is developed.

Carlson and Mack[6] determined empirical relations to relate the attainable leading-edge thrust to various aerofoil geometric parameters, as well as Reynolds and Mach number. Kulfan[7,8] surmised that local leading-edge separation occurs when a profile's leading-edge thrust is equal to its leading-edge drag (giving rise to a separation bubble or, on slender wings, the development of vortex lift). Reference 9 gives an expression for the leading-edge drag, which enables the determination of the incidence at which separation occurs, as well as allowing estimation of the attainable thrust, and on slender wings—the vortex lift. To utilize either of these approaches a theoretical distribution of leading-edge thrust is required. This is usually determined by computational methods. It is, however, desirable for the purposes of preliminary design, to have simple analytic expressions for estimates of lift and drag of slender planar delta wings where the leading edges are not necessarily sharp, and where nonlinear effects can be accounted for.

Incompressible expressions for lift and drag are derived for basic and cropped delta wings. Separate expressions are determined based on the empirical relations of Ref. 6, and the method of Kulfan.[7,8] The expressions are evaluated and compared with experimental results.

Discussion of Method

To determine the attainable leading-edge thrust, an expression is required for the theoretical spanwise thrust distribution. As a simplifying assumption the distribution will be assumed to be linear (being zero at the wing root, and a maximum at the wingtip). This will generally result in an overestimation of attainable thrust inboard, and an underestimation outboard. Combining this assumed theoretical thrust distribution with the Ref. 1 expression for the total theoretical leading-edge thrust given by

$$C_T = (k_p - k_p^2 k_i)\sin^2\alpha \tag{1}$$

where $k_i = \partial C_{Di}/\partial C_T^2$, gives the spanwise thrust distribution as

$$c_t = 6b\eta(k_p - k_p^2 k_i)\sin^2\alpha/[ARc_R(1 + 2\lambda)] \tag{2}$$

Estimation of the Effective Thrust—Method 1

To determine the effective wing thrust, it will be assumed that partial separation has occurred from the wingtip to an arbitrary inboard position. From the wingtip to this point the thrust is equal to the attainable thrust, and from this point inboard, the theoretical thrust. The actual point would be that at which the attainable thrust equals the theoretical thrust (i.e., η_T), and is given by

$$\eta_T = \frac{ARc_R(1 + 2\lambda)\dfrac{c_n}{c}\dfrac{\tau_n}{c_n}\left(\dfrac{r_n}{c_n}\right)^{0.4}\cos^2\Lambda_{LE}}{6b(k_p - k_p^2 k_i)\sqrt{1 - M_n^2}\sin^2\alpha}\left[\frac{2(1 - M_e^2)}{M_e}\right]^{10/6} \tag{3}$$

The parameters M_e, M_n, c_n/c, τ_n/c_n, and r_n/c_n are assumed to be constant, and are defined in Ref. 6 by Eqs. (2), (5), (6), (7), and (8), respectively. The Reynolds number used to evaluate M_e [Ref. 6 Eq. (2) and, hence, Eq. (4)] is that at the wing's mean aerodynamic chord. This is used as incorporation of the spanwise variation of Reynolds number leads to excessive complication in the integral describing the attainable leading-edge thrust. This is not expected to introduce an excessive error, as the dependence of the limiting pressure (and hence M_e) on Reynolds number for a given Mach number is weak.[6] The effective thrust is then determined by integrating the sectional theoretical thrust from the wing root to η_T, and the sectional attainable thrust from η_T to the wingtip. The attainable thrust was estimated using Ref. 6 Eq. (3) (the fraction of theoretical thrust attainable) and Eq. (2) derived previously. This yields

$$\begin{aligned} C_{T_{\text{eff}}} &= \frac{6(k_p - k_p^2 k_i)}{(1 + 2\lambda)}\left[\frac{\eta_T^2}{2} + \frac{\eta_T^3}{3}(\lambda - 1)\right]\sin^2\alpha \\ &+ \frac{b}{S}c_R\frac{2(1 - M_e^2)}{M_e}\left(\frac{c_n}{c}\right)^{0.6}\cos^{1.2}\Lambda_{LE}\left[\frac{\dfrac{\tau_n}{c_n}\left(\dfrac{r_n}{c_n}\right)^{0.4}}{\sqrt{1 - M_n^2}}\right]^{0.6} \\ &\times \left[\frac{6b(k_p - k_p^2 k_i)}{ARc_R(1 + 2\lambda)}\right]^{0.4}\left\{\frac{25 + 35\lambda}{84}\right. \\ &\left. - \left[\frac{\eta_T^{1.4}}{1.4} + \frac{\eta_T^{2.4}}{2.4}(\lambda - 1)\right]\right\}\sin^{0.8}\alpha \end{aligned} \tag{4}$$

The first term on the right of Eq. (4) represents the theoretical (or attached) thrust contribution, and the second term the attainable thrust (partial flow separation present). k_i and k_p may be evaluated using lifting surface theory.

Estimation of the Effective Thrust—Method 2

Kulfan[7,8] assumed that flow separation started at an angle of attack at which leading-edge drag equals leading-edge thrust. On aerofoils this corresponds to the onset of laminar separation, and on slender wings vortex separation. Reference 9 suggests an expression for leading-edge drag (for incompressible flow), which when equated to Eq. (2) yields the spanwise position of separation for a given angle of attack as

$$\eta_s = \frac{\pi}{6b}\left(\frac{r}{c}\right)\frac{\cos\Lambda_{LE}ARc_R(1 + 2\lambda)}{(k_p - k_p^2 k_i)\sin^2\alpha} \tag{5}$$

The attainable thrust was estimated using Ref. 6 definition of the vortex force being equal to the undeveloped thrust. However, instead of the attainable thrust being known (as in method 1), the vortex force is known. This then allows estimation of the effective leading-edge thrust

$$\begin{aligned} C_{T_{\text{eff}}} &= C_T - \frac{6(k_p - k_p^2 k_i)}{(1 + 2\lambda)}\left\{\sin^2\alpha\left[\frac{1}{2} - k_1 + k_1\eta_s\right.\right. \\ &\left. - \frac{\eta_s^2}{2} + (\lambda - 1)\left(\frac{1}{3} - \frac{k_1}{2} + \frac{k_1\eta_s^2}{2} - \frac{\eta_s^3}{3}\right)\right] \\ &+ \cos^2\alpha\left[k_1 - k_1\eta_s + (\lambda - 1)\left(\frac{k_1}{2} - \frac{k_1\eta_s^2}{2}\right)\right] \\ &+ \sin 2\alpha\left[\frac{-2}{3k_1}(k_1 - k_1^2)^{3/2} - \sqrt{k_1}(\lambda - 1)\right. \\ &\times \left.\left(\frac{2}{3}(1 - k_1)^{3/2} - \frac{4}{15}(1 - k_1)^{5/2}\right)\right] \\ &+ \sin 2\alpha\left[\frac{2}{3k_1}(\eta_s k_1 - k_1^2)^{3/2} + \sqrt{k_1}(\lambda - 1)\right. \\ &\left.\left. \times \left(\frac{2}{3}\eta_s(\eta_s - k_1)^{3/2} - \frac{4}{15}(\eta_s - k_1)^{5/2}\right)\right]\right\} \end{aligned} \tag{6}$$

where

$$k_1 = \frac{\pi}{6b}\left(\frac{r}{c}\right)\frac{\cos\Lambda_{LE}ARc_R(1 + 2\lambda)}{(k_p - k_p^2 k_i)} \tag{7}$$

The second term of Eq. (6) divided by $\cos\Lambda_{LE}$ gives the vortex force coefficient.

If the delta wing is cropped, it is necessary to account for the side-edge suction force contribution towards lift and drag. Purvis,[4] using an assumed elliptical spanwise pressure load distribution, suggests an expression for the side-edge suction for both wingtips as

$$C_{SE} = 4.91924(\lambda c_R/b)(k_p^2/\pi AR)\sin^2\alpha\cos^2\alpha \tag{8}$$

From the definition of the potential constant,[1,2] the attached flow normal force coefficient is

$$C_N = k_p \sin\alpha\cos\alpha \tag{9}$$

Having expressions for the overall effective thrust, theoretical thrust, side-edge suction force, and the normal force coefficient, the overall lift and drag properties can be determined.

The total lift is given by

$$\begin{aligned} C_L &= C_{T_{\text{eff}}}\sin\alpha + C_N\cos\alpha \\ &+ \frac{C_T - C_{T_{\text{eff}}}}{\cos\Lambda_{LE}}\cos\alpha + C_{SE}\cos\alpha \end{aligned} \tag{10}$$

The total (inviscid) lift dependent drag is given by

$$\begin{aligned} C_{Di} &= -C_{T_{\text{eff}}}\cos\alpha + C_N\sin\alpha \\ &+ \frac{C_T - C_{T_{\text{eff}}}}{\cos\Lambda_{LE}}\sin\alpha + C_{SE}\sin\alpha \end{aligned} \tag{11}$$

It must be emphasized that η_T and η_v can obviously not be greater than 1. If in evaluation of Eqs. (10) and (11) this occurs, this parameter is put equal to one, indicating that the flow is fully attached along the wing leading edge. The second last term of Eqs. (10) and (11) gives the vortex lift and drag in a formulation suggested in Ref. 6, where the vortex force was equated to the undeveloped leading-edge thrust.

Comparison with Experiment

The results for C_D are presented as a function of angle of attack rather than in $C_D - C_L$ polar form. It is suggested that this provides a better estimate of the accuracy of the method than a drag polar (when the expressions evaluated are a function of angle of attack), where an overestimation of both lift and drag at a specific angle of attack can fortuitously lead to an accurate prediction of drag as a function of lift. The two methods for estimating the attainable thrust are compared with experimental results[10] obtained for a delta wing with a leading-edge sweep angle of 63 deg ($AR = 2$). This wing was also cropped and comparisons are made for a taper ratio of 0.2 giving an aspect ratio of 1.33. The wind-tunnel tests were run at a freestream Mach number of 0.6 corresponding to a Reynolds number of 1.85×10^6 based on the wings mean aerodynamic chord (for $\lambda = 0$). The wings used NACA 63A002 and 63A004 profiles. Figures 1 and 2 show lift and drag of the present methods, and experimental results. Also included are cases for no leading-edge thrust plus vortex lift (i.e., Polhamus) and full leading-edge thrust. Full leading-edge thrust was evaluated by putting the effective thrust equal to the theoretical thrust. The data shows that both methods are in agreement and estimate lift and drag reasonably well up to an angle of attack of about 13 deg, from where these coefficients are overestimated. The same effects (of overestimation of lift, and as a result, drag) were noted in Ref. 1 for a similar aspect ratio sharp-edged delta. These effects were ascribed to trailing-edge separation and vortex breakdown, as

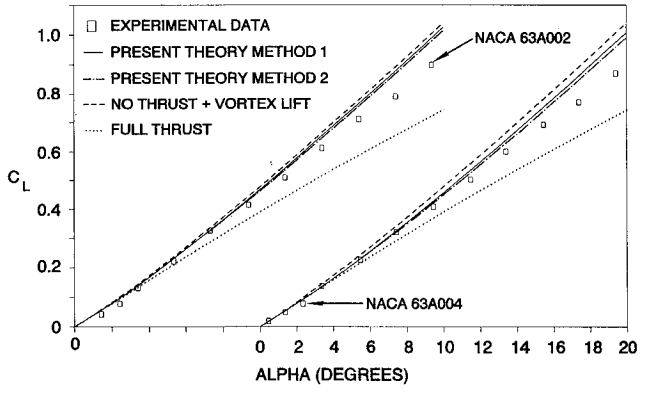

Fig. 1 Comparison of theory and experiment for $AR = 2$, $\lambda = 0$.

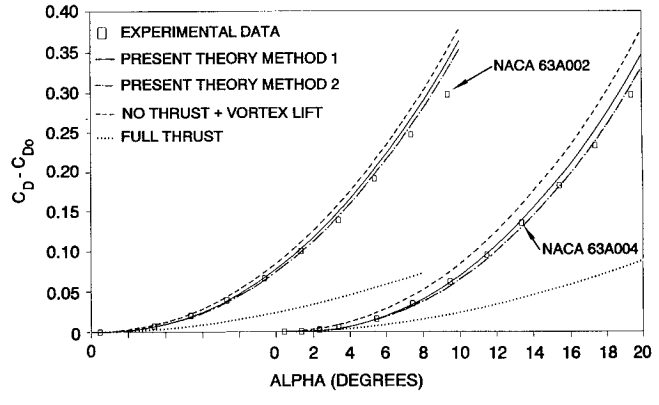

Fig. 2 Comparison of theory and experiment for $AR = 2$, $\lambda = 0$.

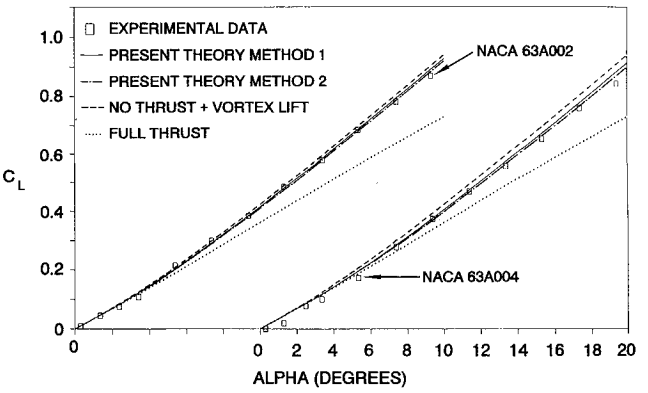

Fig. 3 Comparison of theory and experiment for $AR = 1.33$, $\lambda = 0.2$.

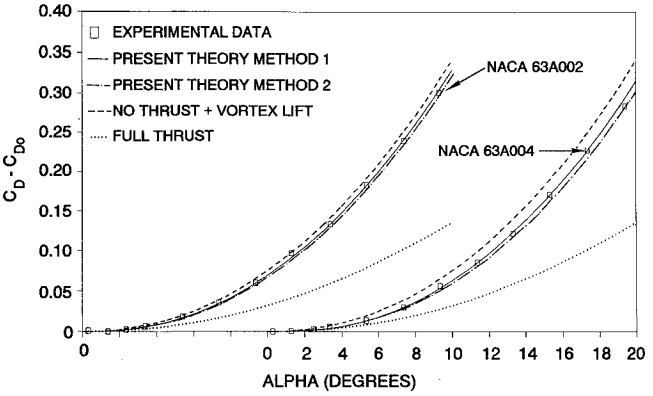

Fig. 4 Comparison of theory and experiment for $AR = 1.33$, $\lambda = 0.2$.

well as insufficient area for full vortex lift recovery. Er-El and Yitzhak[11] showed in an experimental examination of the leading-edge suction analogy, that for high aspect ratio delta wings ($AR > 2$) the overprediction of lift was essentially due to an overestimation of the attached flow normal force coefficient, and not an overprediction of vortex lift. It would thus be expected that the agreement of the present methods with experimental results would extend to higher angles of attack as wing aspect ratio reduces. Figures 3 and 4 show lift and drag for a taper ratio of 0.2 ($AR = 1.33$). Good agreement for both lift and drag is shown to approximately 18-deg angle of attack from where the wings begin to stall.

Summary

Expressions were derived to analytically determine the lift and drag properties of delta wings with partial leading-edge thrust in subsonic flow. The method uses the suction analogy, with an assumed theoretical leading-edge thrust distribution. Separate expressions to estimate the effective thrust based on the empirical method of Carlson and Mack[6] and the method of Kulfan[7,8] were derived. Some aerofoil and wing geometric parameters, as well as the potential constant, are required in the equations. The two methods were compared with experimental results, and good agreement was shown at moderate angles of attack, this agreement improving as the wing aspect ratio was reduced.

References

[1]Polhamus, E. C., "A Concept of the Vortex Lift of Sharp Edged Delta Wings Based on a Leading Edge Suction Analogy," NASA TN D-3767, Oct. 1966.

[2]Polhamus, E. C., "Predictions of Vortex Lift Characteristics by a Leading-Edge Suction Analogy," *Journal of Aircraft*, Vol. 8, No. 4, 1971, pp. 193–199.

[3]Bradley, R. G., Smith, C. W., and Bhately, I. C., "Vortex-Lift

Prediction for Complex Wing Planforms," *Journal of Aircraft*, Vol. 10, No. 6, 1973, pp. 379–381.

[4]Purvis, J. W., "Analytical Prediction of Vortex Lift," *Journal of Aircraft*, Vol. 18, No. 4, 1981, pp. 225–230.

[5]Kandil, O. A., Mook, D. T., and Nayfeh, A. H., "Nonlinear Prediction of Aerodynamic Loads on Lifting Surfaces," *Journal of Aircraft*, Vol. 13, No. 1, 1976, pp. 22–28.

[6]Carlson, H. W., and Mack, R. J., "Studies of Leading-Edge Thrust Phenomena," *Journal of Aircraft*, Vol. 17, No. 12, 1980, pp. 890–897.

[7]Kulfan, R. M., "Wing Airfoil Shape Effects on the Developments of Leading-Edge Vortices," AIAA Paper 79-1675, Aug. 1979.

[8]Kulfan, R. M., "Wing Geometry Effects on Leading-Edge Vortices," AIAA Paper 79-1872, Aug. 1979.

[9]Robinson, A., and Laurmann, J. A., *Wing Theory*, Cambridge Univ. Press, New York, 1956.

[10]Emerson, H. F., "Wind Tunnel Investigation of the Effect of Clipping the Tips of Triangular Wings of Different Thickness, Camber, and Aspect Ratio—Transonic Bump Method," NACA TN 3671, Dec. 1953.

[11]Er-El, J., and Yitzhak, Z., "Experimental Investigation of the Leading-Edge Suction Analogy," *Journal of Aircraft*, Vol. 25, No. 3, 1988, pp. 195–199.

Computational Study of Plume-Induced Separation on a Hypersonic Powered Model

L. D. Huebner*
NASA Langley Research Center, Hampton, Virginia 23681

Introduction

THE study discusses the computation of hypersonic airbreathing vehicle flowfields under simulated powered conditions. Specifically, this involves performing two-dimensional parabolized Navier-Stokes (PNS) and full Reynolds-averaged Navier-Stokes (RANS) calculations to predict the possible existence and effects of flow separation on the cowl of a hypersonic airbreathing model employing scramjet exhaust flow simulation at representative Mach 10 wind-tunnel conditions. This effect can occur at high enough values of the nozzle pressure ratio (NPR), defined as the ratio of the jet total to freestream pressure, where the plume developed from the internal nozzle expands into the aftbody region far enough away from the body that it causes a reverse flow in the boundary layer on the outside surface of the cowl (Fig. 1). This reverse flow can subsequently cause vortex formation and a separation of the boundary layer, which can be large enough to produce a separation-induced compression. Cowl flow separation under simulated powered conditions has been experimentally documented and computationally predicted.[1] However, its impact on model external aerodynamic forces and moments was not addressed. Flow separation near the cowl of a single expansion ramp nozzle was also predicted by Ruffin et al.,[2] but was said to have been caused by the curvature of the cowl near the trailing edge. Nevertheless, the separation could have been exacerbated by the presence of the plume.

Received June 8, 1993; revision received March 15, 1994; accepted for publication March 22, 1994.

*Aerospace Engineer, Hypersonic Airbreathing Propulsion Branch, Gas Dynamics Division, M/S 413. Senior Member AIAA.

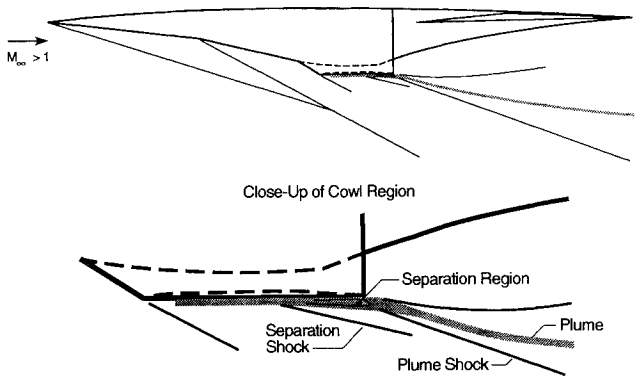

Fig. 1 Plume-induced separation phenomena.

It is the purpose of this Note to present the effects of plume-induced separation, in terms of flowfield features, surface pressures, and potential thermal concerns, using computational fluid dynamics (CFD).

General Aerodynamic Simulation Program 2.0 Attributes Employed

This study was part of a paper discussing the development of the CFD code known as the General Aerodynamic Simulation Program (GASP 2.0), which was the computational code used for this study.[3] Since this problem involves the possible existence and effects of cowl flow separation, both space marching (using the PNS equations) and global iterations (using the RANS equations) were performed independently. The PNS equations are not cast to predict streamwise separation; however, the RANS equations are able to predict streamwise separation. For this study a two-species chemistry model was created using the data base manager within GASP. This new model consisted of a mixture of two different perfect gases, one for the external flow (perfect gas air), and one for the internal flow (a perfect gas with a reduced ratio of specific heats and molecular weight corresponding to that of a noncombusting simulant gas used in powered hypersonic model wind-tunnel testing).[4] The multizone discretization was used to independently begin the external and internal flows and allow them to mix downstream.

Grid Details and Problem Initialization

The domain of the computational space is restricted to below the lower surface centerline of a generic hypersonic model. The geometry contains a faired-over inlet, similar to the type used in powered hypersonic wind-tunnel models. The effects of fairing over the inlet are extremely difficult to address experimentally, but a computational study was performed to assess the effects of inlet fairings.[5] The results of this fairing study showed only small surface pressure differences that were isolated to the region near the cowl leading edge, and that different fairings had little or no impact on lower surface aftbody pressures.

The computational forebody surface has an initial compression angle of 5 deg until the fairing begins about 27 cm downstream of the nose. The fairing adds about 10 deg of compression to the forebody flow. The flat cowl extends from the cowl leading edge (42.5 cm from the nose) to the cowl trailing edge, located about 53.5 cm from the nose. The initial nozzle expansion angle begins at the combustor exit and is approximately 20 deg. It transitions to a 10-deg expansion about halfway down the aftbody, which it maintains to the end of the vehicle, about 85 cm from the nose.

The three zones that comprise this grid are the internal nozzle zone, the forebody/inlet fairing/external cowl zone, and the aftbody zone (beyond the cowl trailing edge where the internal and external flows merge). Grid point connec-